Volume 16
Number 3
21 January 2025
Pages 983–1470

Chemical Science

rsc.li/chemical-science

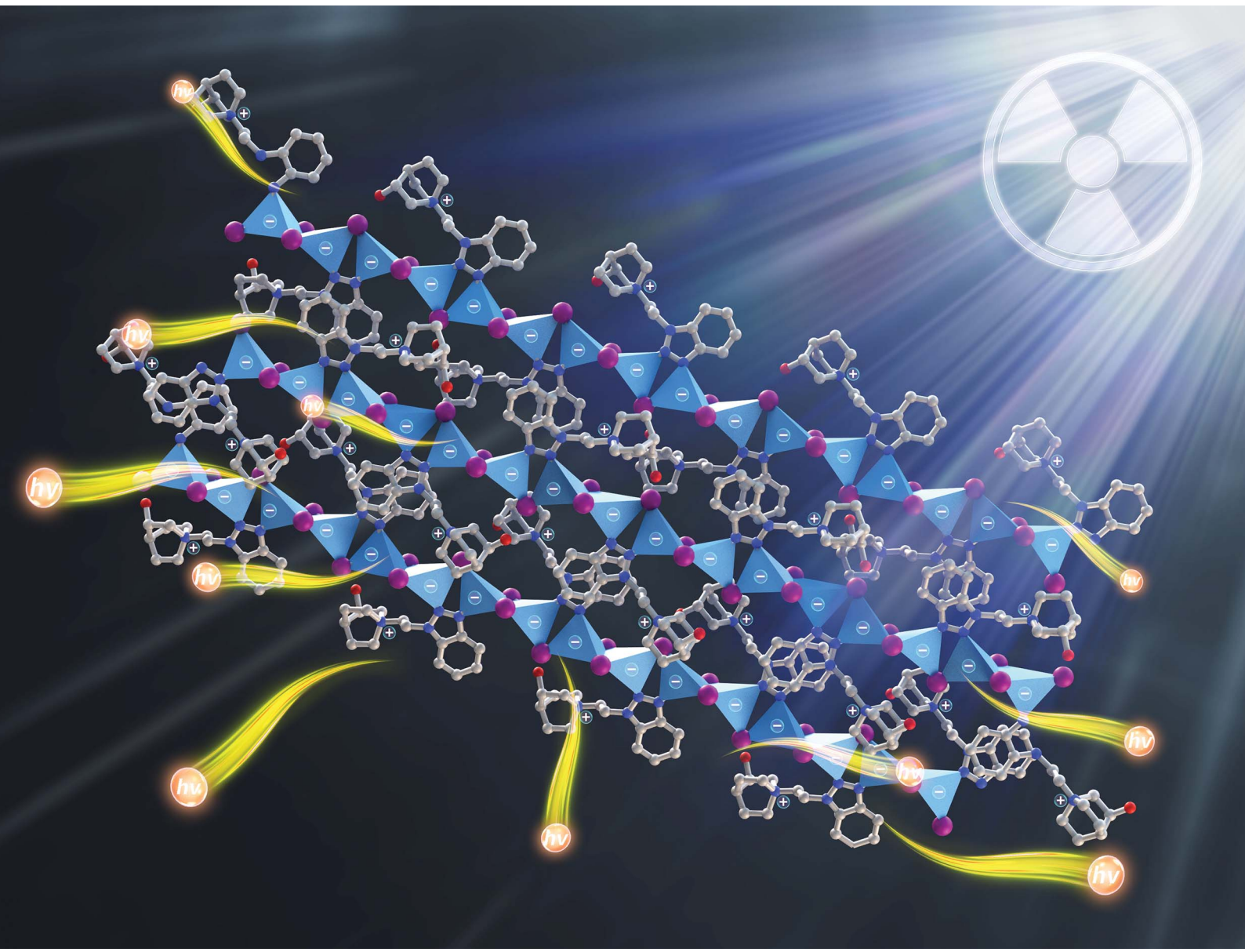

ISSN 2041-6539

ROYAL SOCIETY OF CHEMISTRY

EDGE ARTICLE
Guozhong Xu, Xiuze Hei, Jing Li *et al.*
Strongly photoluminescent and radioluminescent copper(I) iodide hybrid materials made of coordinated ionic chains

15 YEARS ANNIVERSARY

Chemical Science

ROYAL SOCIETY OF CHEMISTRY

EDGE ARTICLE

View Article Online
View Journal | View Issue

Open Access Article. Published on 19 November 2024. Downloaded on 11/15/2025 9:37:27 AM.
This article is licensed under a Creative Commons Attribution-NonCommercial 3.0 Unported Licence.

Check for updates

Cite this: *Chem. Sci.*, 2025, **16**, 1106

All publication charges for this article have been paid for by the Royal Society of Chemistry

Strongly photoluminescent and radioluminescent copper(I) iodide hybrid materials made of coordinated ionic chains†

Jingwen Chen,[ab] Kang Zhou,[b] Jingbai Li,[b] Guozhong Xu,*[a] Xiuze Hei*[b] and Jing Li *[cb]

Received 14th September 2024
Accepted 18th November 2024

DOI: 10.1039/d4sc06242f

rsc.li/chemical-science

Scintillation-based X-ray detection has been widely used in various fields from medical diagnostics to security. In this study, we report four new CuI-based hybrid materials consisting of anionic inorganic chains coordinated to cationic ligands. Due to their unique bonding nature, these compounds demonstrate high stability, solution processability, and efficient photoluminescence with photoluminescence quantum yields (PLQYs) reaching ~85%. Their X-ray scintillation properties are characterized by high light yield comparable to that of commercially available scintillators, an excellent linear response to the X-ray dose rate, a low detection limit, and radio-robustness. In addition, the emission mechanisms and structure–property relationships are also analyzed using both experimental and theoretical methods. These findings suggest possibilities for developing new and high-performance CuI-based hybrid materials for efficient radiation detection and imaging.

Introduction

Copper(I) halide based hybrid materials have garnered increasing interest due to their remarkable structural diversities, excellent luminescence properties, facile synthesis, and non-toxic nature.[1–5] Recent studies have demonstrated the substantial promise of these materials in photoluminescence (PL) related applications, such as light-emitting diodes (LEDs),[6,7] luminescent solar concentrators (LSCs),[8] and X-ray scintillators.[9,10] Comprising both organic and organic components, these hybrid materials combine the advantages of each, thus allowing for fine-tuning of their properties by varying the components. Intriguingly, the inorganic/organic interactions often lead to synergistic features that are extrinsic to both components.[11,12]

Based on the bonding nature between the inorganic and organic motifs, CuX-based hybrid structures can be classified into three subgroups. Subgroup 1 (or Type-I) compounds consist of charge neutral organic and inorganic components that are connected *via* coordinate/dative bonds only;[13,14] subgroup 2 (or Type-II) compounds are characterized by cationic organic and anionic inorganic motifs that form pure ionic bonds;[15,16] subgroup 3 (or Type-III) compounds are essentially a combination of Type-I and Type-II structures and they are also referred to as All-In-One (AIO) structures.[17–20] Different from Type-I and Type-II compounds, they are made of anionic inorganic motifs $(Cu_mI_{m+n})^{n-}$ and cationic organic ligands (L^{k+}) that are further coordinated by dative bonds. The unique bonding characteristics of AIO compounds provide them with intriguing properties and are of particular interest. By integrating both dative bonds (as seen in Subgroup 1) and ionic bonds (as seen in Subgroup 2) at the organic/inorganic interfaces, the resulting AIO compounds inherit beneficial features not only from both components but also from both types of bonds, including structural/optical tunability, strong luminescence, and high solubility and stability.[9,21–24] These desirable features provide the AIO compounds with significantly broadened applicability that would be difficult to achieve by either subgroup alone.

Scintillators, which emit low-energy visible photons in response to ionizing radiation such as X-rays, have received extensive attention recently due to their potential in radiation detection for security inspection, medical imaging, and X-ray astronomy.[25–27] While various types of materials have been exploited, many still face significant limitations, making the search for low-cost and efficient scintillation materials a matter of great scientific and practical importance.[28] Inspiration comes from the AIO compounds. These compounds consist of anionic $(Cu_mI_{m+n})^{n-}$ modules that are coordinated to cationic ligands. With the presence of heavy atoms such as Cu and particularly I

[a]College of Chemical Engineering, University of Science and Technology Liaoning, Anshan 114051, China. E-mail: gz_xu@ustl.edu.cn

[b]Hoffman Institute of Advanced Materials, Shenzhen Polytechnic University, 7098 Liuxian Blvd., Shenzhen, 518055 China. E-mail: xiuzehei@szpu.edu.cn

[c]Department of Chemistry and Chemical Biology, Rutgers University, 123 Bevier Road, Piscataway, NJ 08854, USA. E-mail: jingli@rutgers.edu

† Electronic supplementary information (ESI) available: Methods, ^{1}H NMR spectra, crystal data, structural plots, DFT calculations and photophysical properties. CCDC 2374849–2374852. For ESI and crystallographic data in CIF or other electronic format see DOI: https://doi.org/10.1039/d4sc06242f

© 2025 The Author(s). Published by the Royal Society of Chemistry

Open Access Article. Published on 19 November 2024. Downloaded on 11/15/2025 9:37:27 AM.
This article is licensed under a Creative Commons Attribution-NonCommercial 3.0 Unported Licence.

(Z= 53 for iodine; Z = 29 for copper) in these compounds,[6] they possess high effective atomic numbers that would ensure strong X-ray stopping power (eqn (S1) and (S2)†); additionally, AIO compounds often demonstrate intense photoluminescence, which is advantageous for the efficient conversion of X-ray to visible light (eqn (S3)†);[29] their excellent framework stability and solution processibility also allow for a simple and low-cost fabrication process.

To validate our hypothesis, we designed and synthesized four new AIO compounds made of 1D (one-dimensional) $[Cu_4I_6]_n^{2n-}$ anion chains coordinated with cationic ligands. All compounds demonstrate strong photoluminescence (PL) in the low-energy yellow-orange region (560–610 nm) with the highest PLQY reaching 85%. The emission mechanisms were studied by both theoretical and experimental methods. With the decomposition temperature exceeding 220 °C, all compounds are stable towards heat and moisture. All four compounds exhibit high radioluminescence (RL), similar to their PL, along with excellent linearity, low detection limit and robust radio stability. Our findings indicate that AIO compounds hold great promise as efficient and low-cost scintillation materials.

Results and discussion

Structural description

To obtain AIO structures, the ligands were designed to contain both available coordination sites to ensure the formation of dative bonds with Cu atoms, and cationic centers to introduce ionic interactions.[17,30] Using benzotriazole and 3-quinuclidinol as building blocks, two new cationic ligands were synthesized by a two-step process. The molecular structures of these ligands are shown in Fig. S1 and S2,† along with ^{1}H NMR confirming their purity. Layered diffusion reactions of the ligands with copper(I) iodide resulted in high-quality single crystals suitable for single-crystal X-ray analysis of four new AIO hybrid compounds. As depicted in Fig. 1 and S6,† all four compounds consist of the same 1D anionic $[Cu_4I_6]_n^{2n-}$ chains that are directly coordinated to the cationic ligands *via* Cu–N bonds, forming overall charge-neutral structures. Important crystallographic data are summarized in Table S1.†

In all structures, Cu atoms are tetrahedrally coordinated to three I atoms and one N atom from the ligands, while all I atoms are bridging to two Cu atoms. The two free binding sites of each ligand are both involved in the coordination, forming a five-member ring with two Cu atoms and a bridging I atom. Such a coordination mode has proven to effectively suppress the molecular motions of ligands such as rotations and vibrations, thereby limiting non-radiative decays.[20,30] The Cu–N bond lengths in all compounds range from 2.0–2.2 Å, consistent with the previously reported structures with Cu–N bonds.[31–33]

Interestingly, polymorphs with the exact same ligands but different ligand arrangements can be obtained by modifying synthesis conditions. For example, in compound **1** the ligands are arranged in a "C" manner (alkyl chains of the ligands on opposite sides are pointed in the same direction when viewed along the chain direction). In compound **2**, however, the same ligands adopt a "Z" configuration, with their alkyl chains pointing in opposite directions (Fig. 1b and c). A similar phenomenon was observed in compounds **3** ("C" configuration) and **4** ("Z" configuration) as well (Fig. 1d and e). Such structural differences may be attributed to the H-bond induced structure directing effect in different solvent systems. Such subtle changes in ligand arrangement also induce variations in structural torsion and inter-chain interactions. The two tetrahedral parameters of Δd (bond distance deviation) and $\Delta\theta$ (bond angle deviations) are calculated according to eqn (S4) and (S5), and are used to quantify the structural deviations of $\{CuI_3N\}$ tetrahedral geometry in bond length and bond angle,

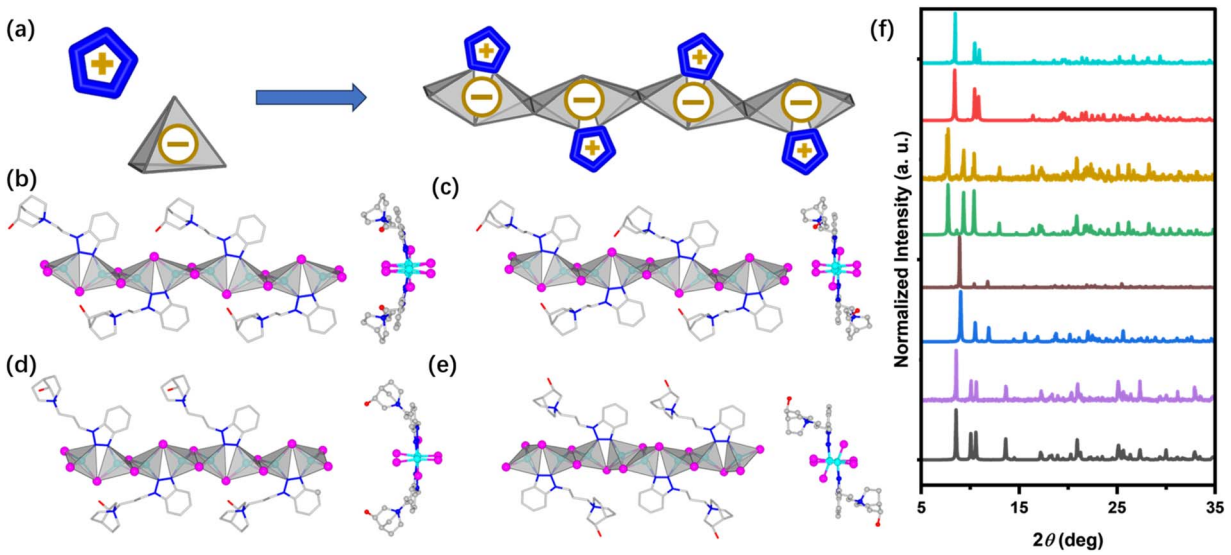

Fig. 1 (a) Schematic showing the construction of 1D-chain AIO structures. Crystal structures of compounds (b) **1**, (c) **2**, (d) **3** and (e) **4**. Color scheme: cyan: Cu; purple: I; gray: C; blue: N; red: O. All H atoms, disorders, and solvated molecules are omitted for clarity. (f) PXRD patterns of all four compounds. From bottom to top: simulated **1**, as made **1**; simulated **2**, as made **2**; simulated **3**, as made **3**; simulated **4**, and as made **4**.

Open Access Article. Published on 19 November 2024. Downloaded on 11/15/2025 9:37:27 AM.
This article is licensed under a Creative Commons Attribution-NonCommercial 3.0 Unported Licence.

Table 1 Important structural parameters of compounds **1–4**[a]

#	Δd ($\times 10^{-3}$)	$\Delta\theta$ ($\times 10^{-3}$)	θ (°)	d (Å)
1	9.937	4.111	11.9	3.37
2	9.737	1.410	19.7	3.35
3	9.673	1.104	23.2	3.31
4	9.722	2.425	21.4	3.37

[a] Δd: bond distance deviation; $\Delta\theta$: bond angle deviation; θ: displacement angle; d: vertical distance.

respectively.[34,35] As shown in Table 1, no obvious difference is observed in Δd. Whereas a more distinct difference of $\Delta\theta$ indicates varying degrees of structural torsion and the Jahn–Teller effect within the structure backbones.[36] For the inter-chain interactions, as shown in Fig. S6,† π–π interactions were observed between two adjacent N-heterocyclic rings from different chains, with their displacement angles (θ) of 12–23° and vertical distances (d) of 3.31–3.37 Å. These numbers are well within the range of strong π–π interactions.

DFT calculations

To gain insights into the electronic structures, the projected density of states (PDOS) of all title compounds was calculated using the VASP.[37] The calculation details can be found in the experimental section. As depicted in Fig. 2, S7 and S8,† all compounds share similar features. While the atomic states that contribute to the valence band maximum (VBM) are mostly from inorganic components (Cu 3d and I 5p orbitals), their conduction band minimum (CBM) is primarily made of C 2p and N 2p orbitals from the cationic ligands. The ligand contributions are dominated by the aromatic π systems. Therefore, the emissions of all compounds are largely associated with the excited states generated from the (metal/halide)-to-ligand charge transfer [(M + X)LCT] process.[38,39]

Interestingly, the influence of the ligand arrangement on their electronic structures has been successfully captured by our calculations. While the VBMs of all title compounds demonstrate negligible differences, their CBMs, despite being composed of the same ligands (in **1** & **2** and **3** & **4**), show distinct characteristics due to the different arrangements of the ligands (Fig. 2, S7 and S8†). In compound **1**, the stronger inter-chain π–π interaction results in bonding characters between the LUMOs of the isolated ligands, and therefore, a slightly lower energy level of its CBM. However, in compound **2**, the interaction is relatively weaker, giving less π–π bonding feature of the CBM with the energy level closer to the LUMO energy of the isolate ligands. As a result, **2** demonstrates a slightly larger band gap compared to compound **1**, which are constructed of the exact same ligands.

Photophysical study

Photoluminescence and diffuse reflectance spectroscopic measurements of all title compounds were conducted at room temperature to investigate their photophysical properties. Upon excitation, all compounds demonstrated intense

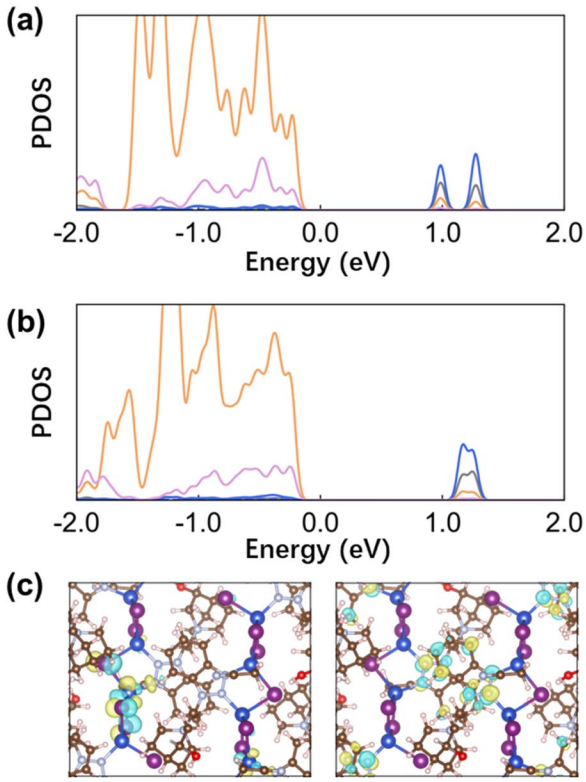

Fig. 2 Calculated projected density of states (PDOS) of compounds (a) **1** and (b) **2**. Color scheme: yellow: Cu 3d; purple: I 5p; blue: N 2p; black: C 2p. (c) The wave functions of the VBM (left) and CBM (right) of compound **1**.

photoluminescence, with their emission peak wavelength ranging from 560 to 610 nm. Their emission colors varied from yellow with Commission International del'Eclairage (CIE) color coordinates (x, y) of (0.44, 0.54) to orange with CIE coordinates of (0.55, 0.44). Broad-band emission profiles were observed for all compounds, with full-width at half-maximum (FWHM) values of approximately 130 nm. This indicates the charge transfer characteristics of their excited states, aligning well with our calculation results and has been observed for many CuI–L based hybrid materials.[40,41] As depicted in Fig. 3c and S9,† along with the excitation wavelength changes, only the changes in emission intensities were observed, while their emission peaks and shapes remained consistent, implying that their emissions originate from a single excitation process. The photoluminescence quantum yields (PLQYs) of all compounds were determined at room temperature (Fig. S10–S13†) under 360 nm excitation, with the highest value of 84.8% of compound **1**, as listed in Table 2. To quantitatively assess their emission efficiencies, total radiative rates (k_r) and non-radiative decay rates (k_{nr}) were estimated based on eqn (1) and (2), where η_{PL} is the PLQY value and τ_{PL} is the average PL lifetime.

$$\eta_{PL} = k_r/(k_r + k_{nr}) \quad (1)$$

$$\tau_{PL} = 1/(k_r + k_{nr}) \quad (2)$$

 © 2025 The Author(s). Published by the Royal Society of Chemistry

Open Access Article. Published on 19 November 2024. Downloaded on 11/15/2025 9:37:27 AM.
This article is licensed under a Creative Commons Attribution-NonCommercial 3.0 Unported Licence.

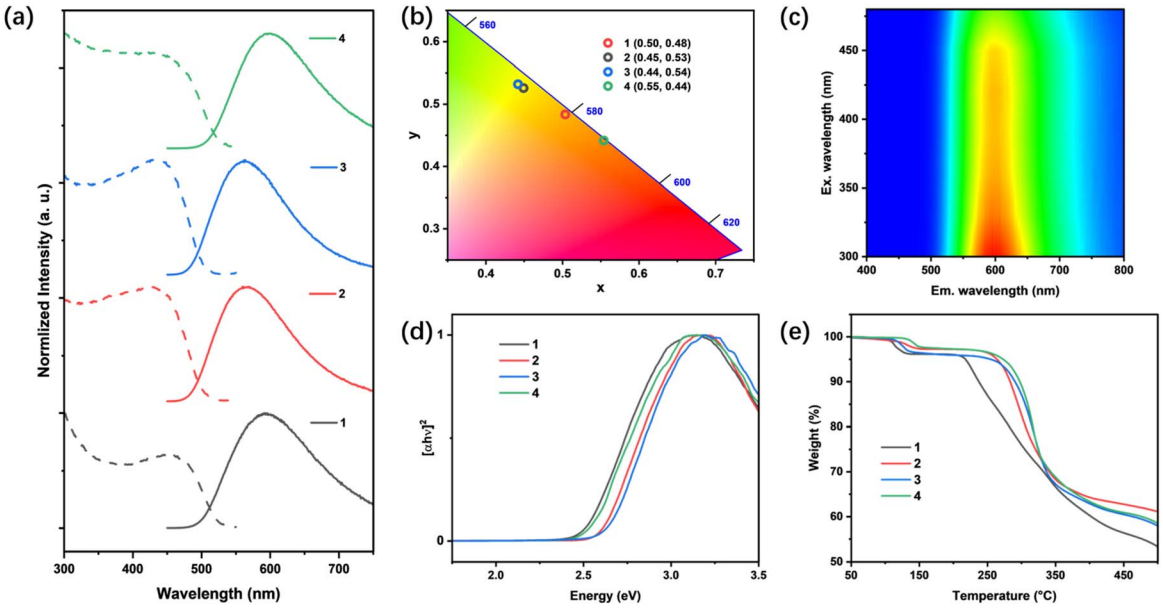

Fig. 3 (a) Normalized PL excitation (PLE, dashed) and PL (solid) spectra and (b) color chromaticity of all title compounds. (c) Excitation-dependent PL spectra of compound **1**. (d) Optical absorption spectra and (e) TG plots of all title compounds.

Table 2 Important photophysical properties of compounds **1**–**4**[a]

#	B. G. (eV)	λ_{em} (nm)	CIE	PLQY[a] (%)	Lifetime (μs)	k_r ($\times 10^4$ s^{-1})	k_{nr} ($\times 10^4$ s^{-1})	T_D[b] (°C)	Solubility[c] (mg mL^{-1})
1	2.5	590	(0.50, 0.48)	84.8	6.15	13.8	2.47	220	80
2	2.6	560	(0.45, 0.53)	67.0	6.54	10.2	5.05	240	60
3	2.5	555	(0.44, 0.54)	66.2	5.07	13.1	6.67	235	90
4	2.6	610	(0.55, 0.44)	71.3	6.46	11.0	4.44	250	100

[a] $\lambda_{ex} = 360$ nm. [b] T_d: decomposition temperature. [c] Test in DMSO at room temperature.

While the k_r of all compounds show subtle differences, the trend of these values (**3** > **2** > **4** > **1**) correlates well with the degree of their overall bond angle deviations $\Delta\theta$ (**3** < **2** < **4** < **1**), implying that the structure torsions induced by differently arranged ligands are responsible for the suppression of non-radiative decay, and thereby leading to higher PLQY.

The optical absorption spectra of all compounds were collected at room temperature using diffuse reflectance spectroscopy (Fig. 3d). Assuming a direct bandgap, the optical band gaps of all compounds were estimated from the absorption edges using the Tauc method, with values ranging from 2.5 to 2.6 eV. These values are consistent with the calculated band gaps of all compounds, though they are slightly larger. This discrepancy is likely due to the delocalization errors in the density functional approximations of the DFT calculations.[42]

Thermalgravimetric analysis (TGA) was performed to evaluate the thermal stability of all title compounds. All compounds remain stable up to 220 °C (Fig. 3e). The observed weight losses at around 150 °C are attributed to the loss of solvated guest molecules (calc. ∼2–5%). Beyond this temperature the weight losses are associated with the leaving of cationic ligands.[43,44] Generally, the "*C*" shape compounds demonstrate slightly lower resistance towards heat compared to their "*Z*" shape counterparts, possibly due to their less symmetrical and energetically less favorable structures.

Another important feature of AIO compounds is their solution processability. Despite being composed of rigid infinite chains, all title compounds demonstrate good solubility in DMSO, as listed in Table 2. This is distinct from most of the Type-I CuX–L hybrid materials that are well-known to be insoluble in common solvents. Consistent with previous studies on the solvation behavior of AIO compounds,[18,45,46] the differences observed in ^{1}H NMR spectra between the dissolved compounds and free ligands (Fig. S3 and S4†) clearly suggest that such intriguing solubility is largely associated with the introduction of ionic nature. The dissolved species are identified as small fragments of anionic CuI clusters with coordinated cationic ligands. By slow addition of antisolvents or cooling, crystalline compounds can be recovered from the solution, suggesting that solution-processed thin-film fabrication of these compounds is highly feasible.

Temperature-dependent lifetime PL spectroscopy was carried out at various temperatures to gain insights into their emission mechanisms. All title compounds exhibit PL lifetimes

Open Access Article. Published on 19 November 2024. Downloaded on 11/15/2025 9:37:27 AM.
This article is licensed under a Creative Commons Attribution-NonCommercial 3.0 Unported Licence.

that are best fit by using monoexponential functions at different temperatures (Fig. 4 and S14†). The observed lifetimes vary from ~20 μs at 77 K to ~8 μs at 287 K (Table S2†), suggesting that their emissions originate solely from the ^{3}(M + X)LCT excited states with phosphorescence at all temperatures. These data well align with the results from our DFT calculations. Interestingly, while little to no peak shift was observed for compounds **1** & **2** within the tested temperature range (Fig. 4c and d), compounds **3** & **4** demonstrate thermochromism behaviors from 77 K to 287 K, as shown in Fig. S15.† For compound **3**, its PL maximum blue-shifted from 580 nm (at 77 K) to 570 nm (at 287 K). In contrast, compound **4** demonstrates a red-shift from 574 nm at 77 K to 595 nm at 287 K. To elucidate the origins of these interesting behaviors, the Huang–Rhys factor (S) and photon frequency ($\hbar\omega_{\text{photon}}$) were estimated from their FWHMs at different temperatures based on eqn (3).[47]

$$\text{FWHM} = 2.36\sqrt{S}\hbar\omega_{\text{photon}}\sqrt{\cot h\frac{\hbar\omega_{\text{photon}}}{2k_{\text{B}}T}} \quad (3)$$

where k_{B} is the Boltzmann constant and T is the temperature.

As shown in Fig. 4 and S15,† all four compounds exhibit low S (8.7–17.6) and high $\hbar\omega_{\text{photon}}$ (39.5–56.8 meV), which imply their high structural rigidity compared to many other CuX-based hybrid structures,[48,49] which is beneficial for the suppression of non-radiative decay processes. Such high structural rigidity and monoexponential decay curves rule out the possibility of structural changes in 1D-$[Cu_4I_6]_n^{2n-}$ chains induced by thermal energy. Therefore, the observed thermochromism is attributed to the inter-chain π–π interactions altered at varied temperatures, leading to consequential changes in the energy level of CBMs. The absence of such thermochromism behavior in compounds **1** & **2** may be attributed to locked chain–chain positions due to more rigid and compact ligand structures.

Radioluminescence study

The solid-state radioluminescence of all title compounds was investigated at room temperature. All title compounds exhibit strong single-band emissions upon X-ray excitation, with the observed RL profiles nearly identical to their PL spectra under UV excitation (Fig. 5b and S17†). This suggests the common origin of their emissions from ^{3}(M + X)LCT excited states. The RL mechanism of these compounds is shown in Fig. 5a. Upon X-ray exposure, the incoming high energy X-ray photons interact with the heavy atoms, specifically Cu and I atoms, through the Compton scattering and photoelectric effect, leading to the ejection of high-energy electrons. These hot electrons consequentially interact with atoms in the materials, losing energy and generating a large number of secondary electrons and eventually electron–hole pairs until sufficient energy has been lost. Finally, the excitons generated settle into ^{3}(M + X)LCT excited states and undergo radiative recombination to yield efficient RL. To quantify their RL light yield, a commercially available scintillation material bismuth germanate (BGO, with a light yield of 10k photon MeV^{-1})[26] was used as a standard reference for quantitative comparison. All measurements were recorded at the same X-ray dose rate, and with the same sample diameter and thickness. The light yields were determined as listed in Fig. 5c, with the highest value of 28.5k photon MeV^{-1}. These values are well in trend with their PLQYs, and are comparable to those of widely investigated pure inorganic

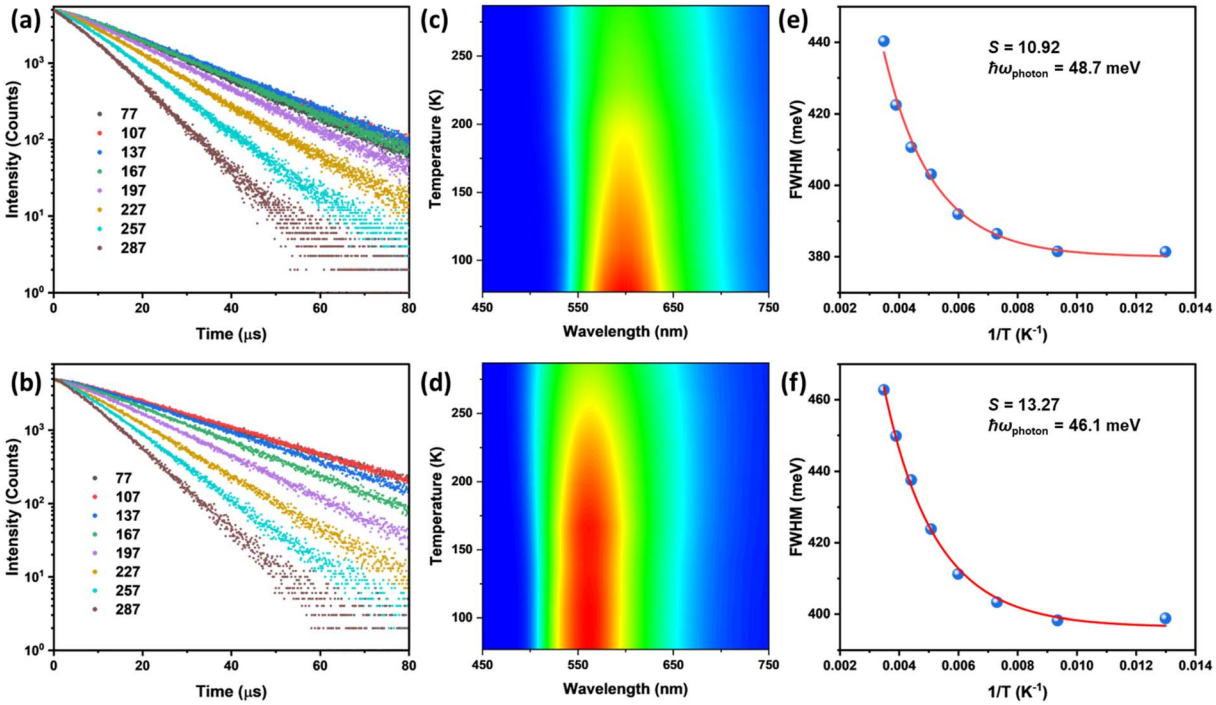

Fig. 4 Photoluminescence decay curves of compounds (a) **1** and (b) **2** at various temperatures. Temperature-dependent PL spectra of compounds (c) **1** and (d) **2**. Huang–Rhys factor (S) and photon frequency ($\hbar\omega_{\text{photon}}$) fitting curves of compounds (e) **1** and (f) **2**.

 © 2025 The Author(s). Published by the Royal Society of Chemistry

Open Access Article. Published on 19 November 2024. Downloaded on 11/15/2025 9:37:27 AM.
This article is licensed under a Creative Commons Attribution-NonCommercial 3.0 Unported Licence.

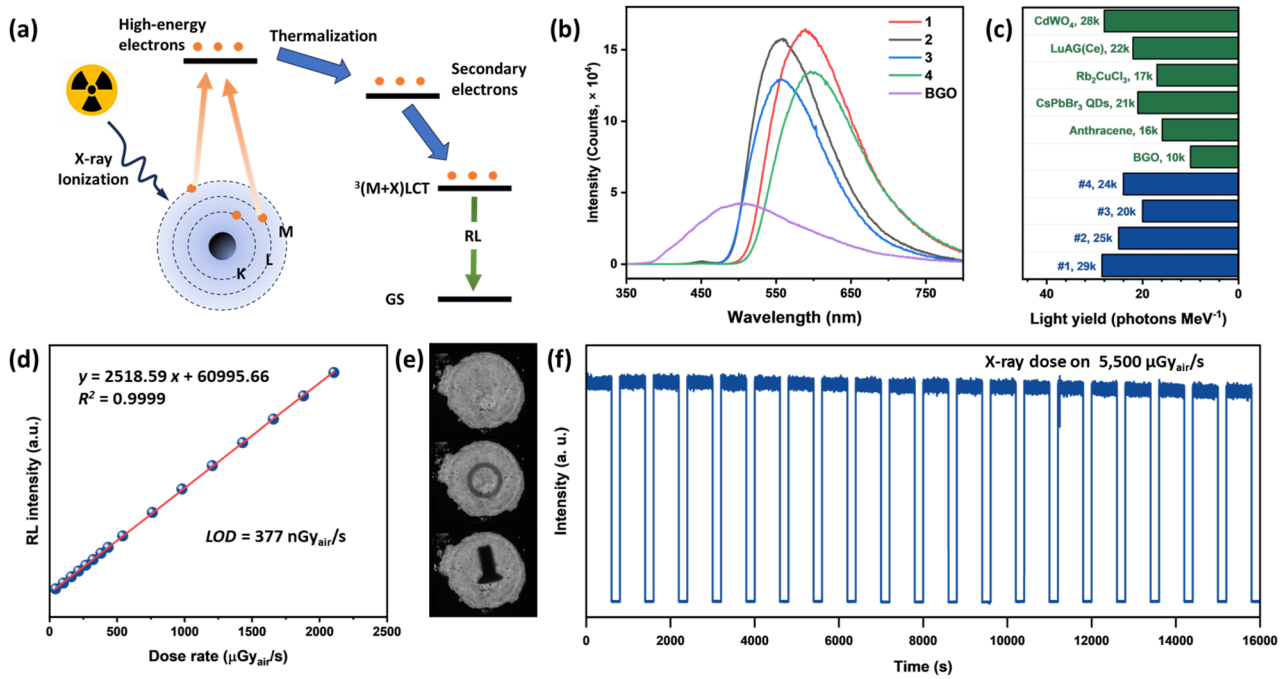

Fig. 5 (a) Schematic of the X-ray scintillation mechanism and (b) radioluminescence spectra of all title compounds and BGO under the exact same test conditions. (c) Comparison of scintillator light yields of compounds **1**–**4** and previously reported and commercially available scintillators; (d) dose rate dependence of the RL intensity of compound **1**; (e) the X-ray images of the AIO pellets (top), with an aluminum ring (middle), and with an iron screw (bottom); (f) the change in the RL intensity under continuous X-ray excitation with a dose rate of 5.5 mGy_{air} s^{-1}.

scintillators Rb_2CuCl_3 (16.6k photon MeV^{-1}),[50] $CsPbBr_3$ QDs (21k photon MeV^{-1}),[51] and commercially available scintillators like $CdWO_4$ (28k photon MeV^{-1}) and LuAG(Ce) (22k photon MeV^{-1}). They are also significantly higher than those of many Type-I (8.7k–15k photon MeV^{-1})[10,52] and Type-II (2.8k–19.9k photon MeV^{-1})[49,53] CuX hybrid structures, demonstrating the promise of these AIO-type materials as scintillators. To evaluate the scintillator response to the X-ray dose rate, compound **1** with the highest light yield was selected to perform X-ray dose rate dependent RL measurement (Fig. 5d). It exhibits excellent linearities to X-ray dose rates in a wide range, from 44 μGy_{air} s^{-1} to 2.1 mGy_{air} s^{-1}. Based on the linearity, the detection limit (DL) of the X-ray dose rate was derived to be 377 nGy_{air} s^{-1} when the signal to noise ratio is 3 using the 3σ/slope method. This DL is 14.6 times lower than the dose rate required for X-ray medical diagnostics (5.5 μGy_{air} s^{-1}).[54]

To further validate the practical use of these compounds as scintillation materials, we pressed compound **1** into a pellet ($\Phi = 1$ cm) as a proof-of concept demonstration. As shown in Fig. 5e, targets of an aluminum ring and an iron screw between the X-ray source and the AIO pellet can be well recognized with clear shapes, and the differences in materials are also reflected by the spatial intensity contrasts, resulting from the different X-ray absorption abilities of Fe and Al. Furthermore, the stability of compound **1** against long-term X-ray exposure was evaluated (Fig. 5f). Even after irradiation under 5.5 mGy_{air} s^{-1}, which is 1000 times higher than the medical diagnostic rate, the compound exhibited negligible loss in RL intensity for more than 4 h, suggesting high resistance towards radio-degradation.

Conclusions

In summary, a series of AIO type CuI-based hybrid materials made of coordinated anionic 1D-$[Cu_4I_6]_n^{2n-}$ chains and cationic ligands have been synthesized and structurally characterized. All compounds demonstrate efficient photoluminescence with low energy emissions (560–610 nm) with their PLQYs up to 84.8%. The emission mechanisms, electronic structures, and structure-property relationship of these materials were investigated both experimentally and theoretically. Moreover, these AIO compounds exhibit high scintillation performance, reaching a RL light yield of 29k photons MeV^{-1} and low X-ray detection limit of 0.377 μGy_{air} s^{-1}. They also show excellent linearity to the dose rate across a wide range and strong resistance towards radio-degradation. These findings highlight the substantial promise of AIO compounds as scintillation materials and offer insights into the development of novel candidates for radiographic applications.

Data availability

The data supporting this article can be found in the ESI.†

Author contributions

Jingwen Chen: data curation, formal analysis, investigation, writing – original draft. Kang Zhou: data curation, formal analysis. Jingbai Li: datacuration, formal analysis, methodology, validation. Guozhong Xu: validation, writing – review & editing, supervision. Xiuze Hei: conceptualization, funding

Open Access Article. Published on 19 November 2024. Downloaded on 11/15/2025 9:37:27 AM. This article is licensed under a Creative Commons Attribution-NonCommercial 3.0 Unported Licence.

acquisition, project administration, validation, writing – review & editing, supervision. Jing Li: project administration, validation, writing – review & editing, supervision.

Conflicts of interest

There are no conflicts to declare.

Acknowledgements

The authors acknowledge the financial support from the Guangdong Basic and Applied Basic Research Foundation (Grant No. 2023A1515110006) and Shenzhen Science and Technology Program (Grant No. 20231124150717002 and No. RCBS20231211090634054).

References

1 X. Hei and J. Li, All-in-one: a new approach toward robust and solution-processable copper halide hybrid semiconductors by integrating covalent, coordinate and ionic bonds in their structures, *Chem. Sci.*, 2021, **12**, 3805–3817.
2 R. Peng, M. Li and D. Li, Copper(I) halides: A versatile family in coordination chemistry and crystal engineering, *Coord. Chem. Rev.*, 2010, **254**, 1–18.
3 J. Troyano, F. Zamora and S. Delgado, Copper(I)–iodide cluster structures as functional and processable platform materials, *Chem. Soc. Rev.*, 2021, **50**, 4606–4628.
4 V. W.-W. Yam, V. K.-M. Au and S. Y.-L. Leung, Light-Emitting Self-Assembled Materials Based on d8 and d10 Transition Metal Complexes, *Chem. Rev.*, 2015, **115**, 7589–7728.
5 X. Zhang, W. Liu, G. Z. Wei, D. Banerjee, Z. Hu and J. Li, Systematic Approach in Designing Rare-Earth-Free Hybrid Semiconductor Phosphors for General Lighting Applications, *J. Am. Chem. Soc.*, 2014, **136**, 14230–14236.
6 N. Zhang, L. Qu, S. Dai, G. Xie, C. Han, J. Zhang, R. Huo, H. Hu, Q. Chen, W. Huang and H. Xu, Intramolecular charge transfer enables highly-efficient X-ray luminescence in cluster scintillators, *Nat. Commun.*, 2023, **14**, 2901.
7 K. Zhu, Z. Cheng, S. Rangan, M. Cotlet, J. Du, L. Kasaei, S. J. Teat, W. Liu, Y. Chen, L. C. Feldman, D. M. O'Carroll and J. Li, A New Type of Hybrid Copper Iodide as Nontoxic and Ultrastable LED Emissive Layer Material, *ACS Energy Lett.*, 2021, **6**, 2565–2574.
8 J.-J. Wang, C. Chen, W.-G. Chen, J.-S. Yao, J.-N. Yang, K.-H. Wang, Y.-C. Yin, M.-M. Yao, L.-Z. Feng, C. Ma, F.-J. Fan and H.-B. Yao, Highly Luminescent Copper Iodide Cluster Based Inks with Photoluminescence Quantum Efficiency Exceeding 98, *J. Am. Chem. Soc.*, 2020, **142**, 3686–3690.
9 Y. Wang, W. Zhao, Y. Guo, W. Hu, C. Peng, L. Li, Y. Wei, Z. Wu, W. Xu, X. Li, Y. D. Suh, X. Liu and W. Huang, Efficient X-ray luminescence imaging with ultrastable and eco-friendly copper(I)-iodide cluster microcubes, *Light: Sci. Appl.*, 2023, **12**, 155.
10 Y. V. Demyanov, Z. Ma, Z. Jia, M. I. Rakhmanova, G. M. Carignan, I. Y. Bagryanskaya, V. S. Sulyaeva, A. A. Globa, V. K. Brel, L. Meng, H. Meng, Q. Lin, J. Li and A. V. Artemev, Copper(I)-Arsine Clusters with a Near-Unity Phosphorescence Quantum Yield for X-Ray Scintillation and LED Applications, *Adv. Opt. Mater.*, 2024, **12**, 2302904.
11 W. Liu, Y. Fang and J. Li, Copper Iodide Based Hybrid Phosphors for Energy-Efficient General Lighting Technologies, *Adv. Funct. Mater.*, 2018, **28**, 1705593.
12 X. Huang, S. Fu, C. Lin, Y. Lu, M. Wang, P. Zhang, C. Huang, Z. Li, Z. Liao, Y. Zou, J. Li, S. Zhou, M. Helm, P. St. Petkov, T. Heine, M. Bonn, H. I. Wang, X. Feng and R. Dong, Semiconducting Conjugated Coordination Polymer with High Charge Mobility Enabled by "4 + 2" Phenyl Ligands, *J. Am. Chem. Soc.*, 2023, **145**, 2430–2438.
13 W. Liu, Y. Fang, G. Z. Wei, S. J. Teat, K. Xiong, Z. Hu, W. P. Lustig and J. Li, A Family of Highly Efficient CuI-Based Lighting Phosphors Prepared by a Systematic, Bottom-up Synthetic Approach, *J. Am. Chem. Soc.*, 2015, **137**, 9400–9408.
14 Y. Fang, W. Liu, S. J. Teat, G. Dey, Z. Shen, L. An, D. Yu, L. Wang, D. M. O'Carroll and J. Li, A Systematic Approach to Achieving High Performance Hybrid Lighting Phosphors with Excellent Thermal- and Photostability, *Adv. Funct. Mater.*, 2017, **27**, 1603444.
15 S. Chen, J. Gao, J. Chang, Y. Li, C. Huangfu, H. Meng, Y. Wang, G. Xia and L. Feng, Family of Highly Luminescent Pure Ionic Copper(I) Bromide Based Hybrid Materials, *ACS Appl. Mater. Interfaces*, 2019, **11**, 17513–17520.
16 G. M. Carignan, S. J. Teat, X. Hei and J. Li, Design, synthesis, structure analysis and photophysical characterization of robust and solution-processable one-dimensional copper(I) iodide-based inorganic-organic hybrid semiconductors, *J. Lumin.*, 2024, **269**, 120435.
17 W. Liu, K. Zhu, S. J. Teat, G. Dey, Z. Shen, L. Wang, D. M. O'Carroll and J. Li, All-in-One: Achieving Robust, Strongly Luminescent and Highly Dispersible Hybrid Materials by Combining Ionic and Coordinate Bonds in Molecular Crystals, *J. Am. Chem. Soc.*, 2017, **139**, 9281–9290.
18 X. Hei, W. Liu, K. Zhu, S. J. Teat, S. Jensen, M. Li, D. M. O'Carroll, K. Wei, K. Tan, M. Cotlet, T. Thonhauser and J. Li, Blending Ionic and Coordinate Bonds in Hybrid Semiconductor Materials: A General Approach toward Robust and Solution-Processable Covalent/Coordinate Network Structures, *J. Am. Chem. Soc.*, 2020, **142**, 4242–4253.
19 X. Hei, S. J. Teat, M. Li, M. Bonite and J. Li, Solution-Processable Copper Halide Based Hybrid Materials Consisting of Cationic Ligands with Different Coordination Modes, *Inorg. Chem.*, 2023, **62**, 3660–3668.
20 X. Hei, S. J. Teat, M. Li, M. Bonite and J. Li, Highly soluble copper(I) iodide-based hybrid luminescent semiconductors containing molecular and one-dimensional coordinated anionic inorganic motifs, *J. Mater. Chem. C*, 2023, **11**, 3086–3094.
21 X. Hei and J. Li, Making coordination networks ionic: a unique strategy to achieve solution-processable hybrid semiconductors, *Mater. Chem. Front.*, 2023, **7**, 4598–4604.

 © 2025 The Author(s). Published by the Royal Society of Chemistry

Open Access Article. Published on 19 November 2024. Downloaded on 11/15/2025 9:37:27 AM.
This article is licensed under a Creative Commons Attribution-NonCommercial 3.0 Unported Licence.

22 L.-Z. Feng, J.-J. Wang, T. Ma, Y.-C. Yin, K.-H. Song, Z.-D. Li, M.-M. Zhou, S. Jin, T. Zhuang, F.-J. Fan, M.-Z. Zhu and H.-B. Yao, Biomimetic non-classical crystallization drives hierarchical structuring of efficient circularly polarized phosphors, *Nat. Commun.*, 2022, **13**, 3339.

23 H. Li, Y. Lv, Z. Zhou, H. Tong, W. Liu and G. Ouyang, Coordinated Anionic Inorganic Module—An Efficient Approach Towards Highly Efficient Blue-Emitting Copper Halide Ionic Hybrid Structures, *Angew. Chem., Int. Ed.*, 2022, **61**, e202115225.

24 A. V. Artem'ev, M. P. Davydova, X. Hei, M. I. Rakhmanova, D. G. Samsonenko, I. Y. Bagryanskaya, K. A. Brylev, V. P. Fedin, J.-S. Chen, M. Cotlet and J. Li, Family of Robust and Strongly Luminescent CuI-Based Hybrid Networks Made of Ionic and Dative Bonds, *Chem. Mater.*, 2020, **32**, 10708–10718.

25 W. Ma, Y. Su, Q. Zhang, C. Deng, L. Pasquali, W. Zhu, Y. Tian, P. Ran, Z. Chen, G. Yang, G. Liang, T. Liu, H. Zhu, P. Huang, H. Zhong, K. Wang, S. Peng, J. Xia, H. Liu, X. Liu and Y. M. Yang, Thermally activated delayed fluorescence (TADF) organic molecules for efficient X-ray scintillation and imaging, *Nat. Mater.*, 2022, **21**, 210–216.

26 L.-J. Xu, X. Lin, Q. He, M. Worku and B. Ma, Highly efficient eco-friendly X-ray scintillators based on an organic manganese halide, *Nat. Commun.*, 2020, **11**, 4329.

27 J.-X. Wang, L. Gutiérrez-Arzaluz, X. Wang, T. He, Y. Zhang, M. Eddaoudi, O. M. Bakr and O. F. Mohammed, Heavy-atom engineering of thermally activated delayed fluorophores for high-performance X-ray imaging scintillators, *Nat. Photonics*, 2022, **16**, 869–875.

28 X. Ou, X. Qin, B. Huang, J. Zan, Q. Wu, Z. Hong, L. Xie, H. Bian, Z. Yi, X. Chen, Y. Wu, X. Song, J. Li, Q. Chen, H. Yang and X. Liu, High-resolution X-ray luminescence extension imaging, *Nature*, 2021, **590**, 410–415.

29 T. Yanagida, G. Okada, T. Kato, D. Nakauchi and S. Yanagida, Fast and high light yield scintillation in the Ga_2O_3 semiconductor material, *Appl. Phys. Express*, 2016, **9**, 042601.

30 X. Hei, K. Zhu, G. Carignan, S. J. Teat, M. Li, G. Zhang, M. Bonite and J. Li, Solution-processable copper(I) iodide-based inorganic-organic hybrid semiconductors composed of both coordinate and ionic bonds, *J. Solid State Chem.*, 2022, **314**, 123427.

31 Y. Fang, C. A. Sojdak, G. Dey, S. J. Teat, M. Li, M. Cotlet, K. Zhu, W. Liu, L. Wang, D. M. ÓCarroll and J. Li, Highly efficient and very robust blue-excitable yellow phosphors built on multiple-stranded one-dimensional inorganic–organic hybrid chains, *Chem. Sci.*, 2019, **10**, 5363–5372.

32 Y. Fang, K. Zhu, S. J. Teat, O. G. Reid, X. Hei, K. Zhu, X. Fang, M. Li, C. A. Sojdak, M. Cotlet and J. Li, Robust and Highly Conductive Water-Stable Copper Iodide-Based Hybrid Single Crystals, *Chem. Mater.*, 2022, **34**(22), 10040–10049.

33 W. Ki, X. Hei, H. T. Yi, W. Liu, S. J. Teat, M. Li, Y. Fang, V. Podzorov, E. Garfunkel and J. Li, Two-Dimensional Copper Iodide-Based Inorganic–Organic Hybrid Semiconductors: Synthesis, Structures, and Optical and Transport Properties, *Chem. Mater.*, 2021, **33**, 5317–5325.

34 K. Robinson, G. V. Gibbs and P. H. Ribbe, Quadratic Elongation: A Quantitative Measure of Distortion in Coordination Polyhedra, *Science*, 1971, **172**, 567–570.

35 Q. Li, Z. Chen, B. Yang, L. Tan, B. Xu, J. Han, Y. Zhao, J. Tang and Z. Quan, Pressure-Induced Remarkable Enhancement of Self-Trapped Exciton Emission in One-Dimensional CsCu2I3 with Tetrahedral Units, *J. Am. Chem. Soc.*, 2020, **142**, 1786–1791.

36 F. Rodríguez, F. Aguado, R. Valiente, M. Hanfland and J. P. Itiè, Variation of the Jahn–Teller distortion with pressure in perovskite layers A2CuCl4. Influence on the charge-transfer band, *Phys. Status Solidi B*, 2007, **244**, 156–161.

37 G. Kresse and J. Furthmüller, Efficient iterative schemes for ab initio total-energy calculations using a plane-wave basis set, *Phys. Rev. B: Condens. Matter Mater. Phys.*, 1996, **54**, 11169–11186.

38 P. Herr, C. Kerzig, C. B. Larsen, D. Häussinger and O. S. Wenger, Manganese(I) complexes with metal-to-ligand charge transfer luminescence and photoreactivity, *Nat. Chem.*, 2021, **13**, 956–962.

39 D. J. Stufkens, Spectroscopy, photophysics and photochemistry of zerovalent transition metal α-diimine complexes, *Coord. Chem. Rev.*, 1990, **104**, 39–112.

40 M. Xie, C. Han, Q. Liang, J. Zhang, G. Xie and H. Xu, Highly efficient sky blue electroluminescence from ligand-activated copper iodide clusters: Overcoming the limitations of cluster light-emitting diodes, *Sci. Adv.*, 2019, **5**, eaav9857.

41 K.-H. Song, J.-J. Wang, L.-Z. Feng, F. He, Y.-C. Yin, J.-N. Yang, Y.-H. Song, Q. Zhang, X.-C. Ru, Y.-F. Lan, G. Zhang and H.-B. Yao, Thermochromic Phosphors Based on One-Dimensional Ionic Copper-Iodine Chains Showing Solid-State Photoluminescence Efficiency Exceeding 99%, *Angew. Chem., Int. Ed.*, 2022, **61**, e202208960.

42 J. Muscat, A. Wander and N. M. Harrison, On the prediction of band gaps from hybrid functional theory, *Chem. Phys. Lett.*, 2001, **342**, 397–401.

43 P. Hao, Y. Qiao, T. Yu, J. Shen, F. Liu and Y. Fu, Three iodocuprate hybrids symmetrically modulated by positional isomers and the chiral conformation of N-benzyl-methylpyridinium, *RSC Adv.*, 2016, **6**, 53566–53572.

44 J.-J. Shen, X.-X. Li, T.-L. Yu, F. Wang, P.-F. Hao and Y.-L. Fu, Ultrasensitive Photochromic Iodocuprate(I) Hybrid, *Inorg. Chem.*, 2016, **55**, 8271–8273.

45 A. V. Artem'ev, E. A. Pritchina, M. I. Rakhmanova, N. P. Gritsan, I. Y. Bagryanskaya, S. F. Malysheva and N. A. Belogorlova, Alkyl-dependent self-assembly of the first red-emitting zwitterionic {Cu4I6} clusters from [alkyl-P(2-Py)3]+ salts and CuI: when size matters, *Dalton Trans.*, 2019, **48**, 2328–2337.

46 X. Hei, S. J. Teat, W. Liu and J. Li, Eco-friendly, solution-processable and efficient low-energy lighting phosphors: copper halide based hybrid semiconductors Cu4X6(L)2 (X = Br, I) composed of covalent, ionic and coordinate bonds, *J. Mater. Chem. C*, 2020, **8**, 16790–16797.

47 W. Stadler, D. M. Hofmann, H. C. Alt, T. Muschik, B. K. Meyer, E. Weigel, G. Müller-Vogt, M. Salk, E. Rupp

Open Access Article. Published on 19 November 2024. Downloaded on 11/15/2025 9:37:27 AM.
This article is licensed under a Creative Commons Attribution-NonCommercial 3.0 Unported Licence.

and K. W. Benz, Optical investigations of defects in Cd1-xZnxTe, *Phys. Rev. B: Condens. Matter Mater. Phys.*, 1995, **51**, 10619–10630.

48 S. Fang, B. Zhou, H. Li, H. Hu, H. Zhong, H. Li and Y. Shi, Highly Reversible Moisture-Induced Bright Self-Trapped Exciton Emissions in a Copper-Based Organic–Inorganic Hybrid Metal Halide, *Adv. Opt. Mater.*, 2022, **10**, 2200605.

49 T. Xu, Y. Li, M. Nikl, R. Kucerkova, Z. Zhou, J. Chen, Y.-Y. Sun, G. Niu, J. Tang, Q. Wang, G. Ren and Y. Wu, Lead-Free Zero-Dimensional Organic-Copper(I) Halides as Stable and Sensitive X-ray Scintillators, *ACS Appl. Mater. Interfaces*, 2022, **14**, 14157–14164.

50 X. Zhao, G. Niu, J. Zhu, B. Yang, J.-H. Yuan, S. Li, W. Gao, Q. Hu, L. Yin, K.-H. Xue, E. Lifshitz, X. Miao and J. Tang, All-Inorganic Copper Halide as a Stable and Self-Absorption-Free X-ray Scintillator, *J. Phys. Chem. Lett.*, 2020, **11**, 1873–1880.

51 Y. Zhang, R. Sun, X. Ou, K. Fu, Q. Chen, Y. Ding, L.-J. Xu, L. Liu, Y. Han, A. V. Malko, X. Liu, H. Yang, O. M. Bakr, H. Liu and O. F. Mohammed, Metal Halide Perovskite Nanosheet for X-ray High-Resolution Scintillation Imaging Screens, *ACS Nano*, 2019, **13**, 2520–2525.

52 Q. Hu, C. Zhang, X. Wu, G. Liang, L. Wang, X. Niu, Z. Wang, W.-D. Si, Y. Han, R. Huang, J. Xiao and D. Sun, Highly Effective Hybrid Copper(I) Iodide Cluster Emitter with Negative Thermal Quenched Phosphorescence for X-Ray Imaging, *Angew. Chem., Int. Ed.*, 2023, **62**, e202217784.

53 D. A. Popy, Y. Singh, Y. Tratsiak, A. M. Cardoza, J. M. Lane, L. Stand, M. Zhuravleva, N. Rai and B. Saparov, Stimuli-responsive photoluminescent copper(I) halides for scintillation, anticounterfeiting, and light-emitting diode applications, *Aggregate*, 2024, **5**, e602.

54 H. Wei, Y. Fang, P. Mulligan, W. Chuirazzi, H.-H. Fang, C. Wang, B. R. Ecker, Y. Gao, M. A. Loi, L. Cao and J. Huang, Sensitive X-ray detectors made of methylammonium lead tribromide perovskite single crystals, *Nat. Photonics*, 2016, **10**, 333–339.

 © 2025 The Author(s). Published by the Royal Society of Chemistry